Spectral Shape of the Two-Photon Decay of the $2\,^1S_0$ State in He-Like Tin

S. Trotsenko,[1,2,3] A. Kumar,[2] A. V. Volotka,[4] D. Banaś,[5] H. F. Beyer,[2] H. Bräuning,[2] S. Fritzsche,[2] A. Gumberidze,[6] S. Hagmann,[1,2] S. Hess,[1,2] P. Jagodziński,[5] C. Kozhuharov,[2] R. Reuschl,[7] S. Salem,[1,2] A. Simon,[8] U. Spillmann,[2] M. Trassinelli,[7] L. C. Tribedi,[9] G. Weber,[2,10] D. Winters,[2] and Th. Stöhlker[2,3,10,*]

[1]*Institut für Kernphysik, Universität Frankfurt, D-60438 Frankfurt, Germany*
[2]*GSI Helmholtzzentrum für Schwerionenforschung, D-64291 Darmstadt, Germany*
[3]*Helmholtz-Institut Jena, D-07743 Jena, Germany*
[4]*Institut für Theoretische Physik, Technische Universität Dresden, D-01062, Dresden, Germany*
[5]*Institute of Physics, Jan Kochanowski University, 25-406 Kielce, Poland*
[6]*ExtreMe Matter Institute EMMI, GSI, D-64291 Darmstadt, Germany*
[7]*Institut des Nanosciences de Paris, CNRS and Université Pierre et Marie Curie-Paris 6, 75015 Paris, France*
[8]*Institute of Physics, Jagiellonian University, Kraków, Poland*
[9]*Tata Institute of Fundamental Research, Mumbai, India*
[10]*Physikalisches Institut, Ruprecht-Karls-Universität Heidelberg, D-69120 Heidelberg, Germany*

(Received 29 June 2008; revised manuscript received 4 August 2009; published 21 January 2010)

The spectral distribution of the $1s2s\,^1S_0 \rightarrow 1s^2\,^1S_0$ two-photon decay of He-like tin was measured using a novel approach at the gas-jet target of the ESR storage ring. Relativistic collisions of Li-like projectiles with low-density gaseous matter have been exploited to selectively populate the desired $1s2s$ state. Compared to conventional techniques, this approach results in a substantial gain in statistical and systematic accuracy, which allowed us to achieve for the first time a sensitivity to relativistic effects on the two-photon decay spectral shape as well as to discriminate the measured spectrum for Sn from theoretical shapes for different elements along the He-isoelectronic sequence.

DOI: 10.1103/PhysRevLett.104.033001 PACS numbers: 32.30.Rj, 31.30.jc, 32.80.Wr

Since the early days of quantum mechanics, the two-photon decay of the $2s_{1/2}$ level of atomic hydrogen has attracted particular interest. While, for hydrogen, a nonrelativistic theory was formulated by Maria Göppert-Mayer [1] already in 1931, a refined treatment for the $1s2s\,^1S_0 \rightarrow 1s^2\,^1S_0$ two-photon decay in helium was provided later by Breit and Teller [2]. In this decay process, two correlated electric-dipole photons with energies $\hbar\omega_1$ and $\hbar\omega_2$ are emitted simultaneously and *share* together the total energy $\hbar\omega$ of the transition: $\hbar\omega_1 + \hbar\omega_2 = \hbar\omega = E_i - E_f$. E_i and E_f refer to the energies of the initial and final states of the transition. The photon energies form a continuous spectrum that is known to have a maximum intensity at half of the transition energy and that falls gradually to zero at both end points of the spectrum, $\hbar\omega_1 = 0$ and $\hbar\omega_1 = E_i - E_f$. In contrast to the one-photon decay, which purely depends on the initial and final states of the transition, the shape of the two-photon continuum is determined by the summation over all intermediate (bound and continuum) states of the atom or ion. Hence, the spectral distribution of the photons is sensitive to the *entire* atomic structure. Therefore, a detailed study of the spectral shape of the two-photon distribution along the helium isoelectronic sequence as the simplest multielectronic system is of great importance for the understanding of the interplay between relativity and electron-electron correlations for medium and high-Z ions. In fact, much theoretical (references in [3]) and experimental [4–8] effort has been spent during the last two decades to accurately determine the spectral properties of the two-photon distribution. Both nonrelativistic and relativistic calculations have been carried out and display differences especially in the full width at half maximum (FWHM) of the spectral shape due to the relativistic ''contraction'' of the wave functions near the nucleus and effects of the electron-electron interaction [9,10].

In this Letter, we describe an experimental study of the spectral distribution of the $1s2s\,^1S_0 \rightarrow 1s^2\,^1S_0$ two-photon decay of He-like tin which utilizes a novel technique. In this study, the $1s2s\,^1S_0$ state is populated via K-shell ionization of the Li-like projectiles in relativistic collisions with a low-density nitrogen target at the heavy-ion storage ring ESR. In Fig. 1, the low-lying levels of He-like tin are displayed together with the dominant transitions and their decay rates. Owing to the high selectivity in producing the $1s2s\,^1S_0$ state [11], the two-photon decay events were registered by a single x-ray detector in coincidence with the He-like charge state after the collision. As a result, a very clean spectral distribution of the photons has been observed, which could be compared with relativistic many-body as well as nonrelativistic calculations. Excellent agreement between experiment and relativistic theory can be stated. When compared with previous measurements of the two-photon decay of He-like Ni [4], Ge [5], Kr [6], and Au [7], the systematic accuracy and acquired statistics of the present measurement are substantially better. Hence, for the first time, the influence of relativistic effects on the $2E1$ spectral shape can be experimentally confirmed.

 © 2010 The American Physical Society

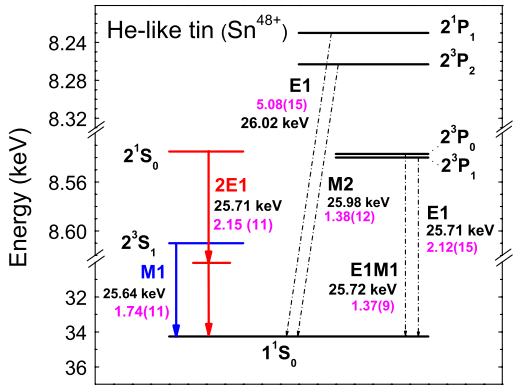

FIG. 1 (color online). Level scheme of Sn^{48+}. The decay modes with their transition energies and decay rates (s^{-1}) are displayed [9,18–20]. The numbers in brackets indicate the power of 10.

In conventional two-photon decay studies, the excited states of He-like ions are produced in collisions with low-Z solid targets, and the x rays are detected by photon-photon coincidence measurements [4,6,7]. Moreover, the photon-photon coincidence technique has often been combined with an additional coincidence on the He-like charge state projectile after the collision. In such cases, electron capture into the projectile has been used as a population process for the $1s2s\,^1S_0$ state. Compared to this, the new method applied in the present study offers several advantages. Most important, the use of a single x-ray detector results in a gain of efficiency by at least 2 orders of magnitude as compared to the x-ray–x-ray coincidence technique. Since the detector setup has no longer to be optimized for high count rate efficiency, small opening angles can now be accepted for the x-ray detection, resulting in a very well-defined geometry. As a consequence, the experiment can be performed with electron-cooled beams at a storage ring using low-density gaseous targets where the relatively large distances between target and detector exclude the application of the x-ray–x-ray coincidence technique. A further advantage related to the use of a single detector is that it substantially improves the control over possible systematic uncertainties. This is the most serious limitation for spectral distribution studies based on the x-ray–x-ray coincidence technique and where the product of the efficiency corrections of both detectors has to be considered. Finally, we would like to emphasize the virtually exclusive population of the $1s2s\,^{1,3}S$ states via K-shell ionization of the initially Li-like ions [11]. Here, unwanted cascade contributions are almost completely suppressed, in contrast to populating the $1s2s\,^1S_0$ state via electron capture or excitation.

The measurements were performed at the experimental storage ring (ESR) at GSI, Darmstadt. The electron-cooled beam of 300 MeV/u Li-like tin ions was incident on a supersonic nitrogen gas-jet target (density $\sim 10^{12}$ atoms/cm^3) [12], and the x rays produced by the ion-atom collisions were registered by a planar high-purity germanium detector placed at an angle of 35° with respect to the beam direction. The detector was separated from the ultrahigh vacuum ($\sim 10^{-11}$ mbar) of the interaction chamber by a 100-μm thick beryllium window. In order to reduce the Doppler broadening of the x-ray lines, a 4-mm-wide copper-lead slit was mounted in front of the detector. After the interaction, the projectile ions that had lost one electron in the collision were separated by the dipole magnet and registered by a multiwire particle detector. The x-ray detector was energy and efficiency calibrated before and after the experiment using ^{57}Co, ^{133}Ba, and ^{241}Am radioisotope sources; see [11] for details about the experimental setup.

In Fig. 2, we display the x-ray spectra of 300 MeV/u Sn^{47+} in collision with nitrogen from the jet target measured *without* (upper part) and *in* coincidence with the He-like ions (lower part). The upper spectrum therefore comprises all x rays from the projectile ions, including those resulting from bremsstrahlung, excitation, ionization, or electron capture, as well as from the fluorescence arising from the collimator slits mounted in front of the detector. Besides this radiation, this spectrum also displays the $2E1$ continuum in the central part. The *pure* $2E1$ spectrum shown in the lower part of Fig. 2 was obtained by detecting the x rays in coincidence with the up-charged (ionized) Sn^{48+} ions. Obviously, this lower spectrum is composed of

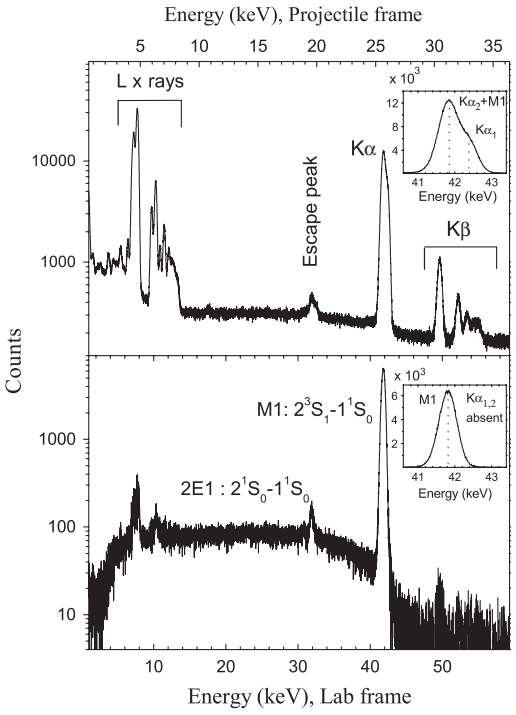

FIG. 2. X-ray spectra of 300 MeV/u Sn^{47+} in collisions with a nitrogen target measured without coincidence (top panel) and in coincidence with up-charged ions (bottom panel) at an angle of 35°. The $K\alpha$ doublet and $M1$ lines and their energy positions are shown in the insets.

the broad continuum of the $2E1$ two-photon decay of the $1s2s\,^1S_0$ level and the intense monoenergetic line due to the $M1$ (single-photon) decay of the $1s2s\,^3S_1$ level (cf. Fig. 1). The absence of further lines arising from the decay of the $2\,^1P_1$ ($E1$ transition) or the $2\,^3P_2$ ($M2$ transition) levels (cf. insets of Fig. 2) suggests that the collisions of the Li-like tin ions with the N_2 target lead to a very selective formation of the single K-shell vacancy, leaving the heliumlike ions either in the $1s2s\,^1S_0$ or the $1s2s\,^3S_1$ level. This finding agrees well with a recent study performed for lithiumlike uranium in which the origin of this high state selectivity was discussed in detail [11].

Owing to the selective ionization of a $1s$ electron, which leaves the $2s$ electron unaffected in its shell, neither the $M1$ line nor the $2E1$ spectral photon distribution is blended by the decay of the $2\,^3P_1$ ($E1$ transition) or $2\,^3P_0$ ($E1M1$ transition) levels, respectively. For the $2\,^3S_1$ level, the $2E1$ to $M1$ branching ratio is 10^{-4} [9] and hence, taking into account the total counts in the $M1$ peak shown in Fig. 2, the $2E1$ decay of the $2\,^3S_1$ level contributes to the $2E1$ spectrum of the $2\,^1S_0$ state by perhaps a few parts per thousand. This small admixture is negligible for the final result. The contributions of the higher multipoles, $2M1$ and $E1M2$, are negligibly small and do not exceed, compared with the $2E1$ channel, 10^{-4} even for $Z = 92$. However, these contributions might become observable in the angular correlation studies of the emitted photons in the future.

Since the "first" photon with energy $\hbar\omega_1$ cannot be distinguished *a priori* from the second one, a symmetric photon distribution is expected with regard to an equal share of energy, $f \equiv \hbar\omega_1/(\hbar\omega_1 + \hbar\omega_2) = 0.50$. In the following, therefore, we can restrict the analysis of the spectral distribution to just one *half* of the energy fraction (cf. Figs. 2 and 3). Since the detector efficiency is very well known at higher photon energies (in the interval 20–45 keV, the relative efficiency is known with an accuracy of better than 1%) and there is no further contamination in this region, we consider in the following always the "upper half" of the spectral distribution, $f \geq 0.5$. For this part, only the low-energy tail of the intense $M1$ line might affect the high-energy end of the $2E1$ spectrum. Therefore, the response function of the Ge detector was simulated with the EGS4 package [13,14]. In the simulation, different photon-atom collision processes in the Ge crystal and the geometrical parameters were considered. The simulation results (bottom part of Fig. 3) have then been convoluted with the energy dependent resolution of the detector and the Doppler broadening due to the finite opening angle of the detector. The detector simulations reproduce the measured position and intensity of the Ge K escape peaks very well, when compared to the $M1$ line intensity (Fig. 3). The low-energy tail of the $M1$ peak extends up to $f = 0.92$ (corresponding to 38.6 keV photon energy in the laboratory frame) (Fig. 3). Therefore, for the part contaminated by the $M1$ decay, we conservatively assume $f \gtrsim 0.92$. The Ge K

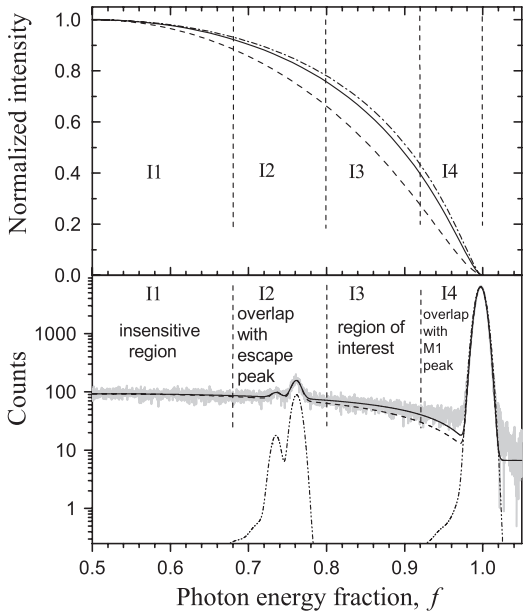

FIG. 3. Top part: higher energy half of the fully relativistic calculated two-photon energy distribution for He-like Ni (dash-dotted line), Sn (solid line), and U (dashed line). Bottom part: comparison of the measured two-photon spectral distribution of He-like tin (solid light gray line) with a fully relativistic calculation for He-like Sn (solid line) and U (dashed line), together with the simulation of the detector response function for the $M1$ line (dotted line).

escape peak rides on the $2E1$ spectral distribution from $f = 0.68$–0.78 (28.5–32.7 keV photon energy in the lab frame).

The observed spectral distribution is compared with fully relativistic computations that are based on a dual-kinetic-balance finite basis set method [15] in order to perform the summation over the complete Dirac spectrum. In these computations, the interelectronic interactions have been taken into account by means of the Kohn-Sham potential. Comparing this approach to Ref. [9], where the relativistic configuration interaction method was employed, the deviation is 1.3% for $Z = 28$ and decreases up to 0.04% as Z is increased to $Z = 92$. From this comparison, we conclude that our approach is adequate for the region $Z = 28$–92 with an uncertainty of about 0.5%–1.5%. To compare the $2E1$ spectral distribution of the heliumlike ions with different nuclear charges Z, the distributions were normalized to $f = 0.50$ (Fig. 3). Moreover, for the following discussion, we subdivide the spectral shape into the three energy intervals: $I1$ [0.50, 0.68] the region insensitive on Z, $I2$ [0.68, 0.8] the region contaminated by the escape peaks, and $I3$ [0.8, 0.92] the "region of interest," respectively (cf. Fig. 3). For comparison with theory, we consider the ratio R given by the number of events registered in the region of interest $I3$ divided by the one found in the insensitive region $I1$, which is not contaminated by the escape lines. In Table I this experimental

TABLE I. Intensity ratio $R =$ "$I3/I1$" (Fig. 3, bottom) for the measured $2E1$ shape of Sn^{48+}, compared with theoretical values for different ions along the He-isoelectronic sequence.

Z	Experiment	Theory		
	He-like	Relativistic[a]	Relativistic[b]	Nonrelativistic
28	···	0.403	0.418	0.416
50	0.390 ± 0.003	0.386	0.396	0.422
60	···	0.374	0.381	0.423
70	···	0.366	0.367	0.424
92	···	0.324	0.329	0.425

[a]With electron-electron correlations.
[b]Without electron-electron correlations.

ratio R is compared with the corresponding theoretical result obtained by an integration over the energy regions of relevance. The experimental ratio is found to be in good agreement with the relativistic theoretical value predicted for heliumlike Sn, especially considering the accuracy of the latter of about 0.5%–1.5% (as explained above). At the same time, the experimental value for Sn obtained in this work significantly departs from theoretical predictions for all the other elements considered in the table. Moreover, our result can unambiguously distinguish between predictions of relativistic and nonrelativistic calculations.

We also performed comparison of the measured spectral shape with the theoretical one using the MINUIT minimization code [16] by requiring the best agreement (minimum χ^2) between the theoretical and measured spectral shapes. In Fig. 4, we present the fraction (experiment − theory)/theory comparing our experimental results with theoretical line shapes for different Z. In the insensitive region, the shapes cannot be distinguished, while the difference is clearly visible for the region of interest ($I3$). Our data points come closest (within $\pm 3\sigma$) to the theoretical spectral shape for Sn, whereas for U the data points start deviating from 0.80 and depart up to several 10σ at $f = 0.92$. This is due to the relativistic effects, making the $2E1$ spectrum for Yb and U substantially narrower as compared to Sn. The conclusion drawn from this comparison of experimental and theoretical shapes is consistent with the results presented in the Table I.

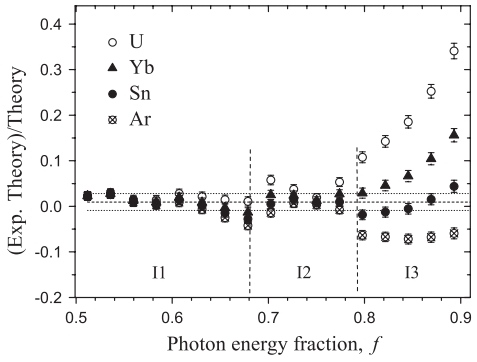

FIG. 4. (Experiment − theory)/theory intensity ratio with theoretical values for Ni, Sn, Yb, and U as a function of the photon energy fraction. Each point corresponds to a bin of 1 keV. Horizontal lines are the mean and $\pm 3\sigma$ values for Sn.

In summary, we have measured the spectral photon distribution from the $1s2s\,^1S_0 \rightarrow 1s^2\,^1S_0$ two-photon decay of He-like tin. The measurements are based on a novel experimental approach in which the desired excited state of the He-like ions is formed selectively by relativistic collisions of Li-like projectiles with gaseous target. Applying this technique to the $2E1$ decay study, we were able to achieve a substantial gain in statistics and overall accuracy as compared to previous studies. Our result unambiguously favors predictions of relativistic many-body theory as compared to the nonrelativistic calculations. The developed method can be utilized for a broad range of new interesting studies. In the future, further experiments will be devoted to the angular correlation and polarization studies in the two-photon decay of high-Z ions where contributions of higher multipoles are expected to cause asymmetries in the photon-photon emission [17].

The support by the DAAD (A. K., No. A/05/52927), Humboldt Foundation (M. T.), Polish Ministry of Education and Science (No. 1P03B00629), and I3 EURONS (EC No. 506065) is gratefully acknowledged. A. V. V. acknowledges useful discussions with V. M. Shabaev.

*t.stoehlker@gsi.de

[1] M. Göppert-Mayer, Ann. Phys. (Leipzig) **401**, 273 (1931).
[2] G. Breit and E. Teller, Astrophys. J. **91**, 215 (1940).
[3] P. H. Mokler and R. W. Dunford, Phys. Scr. **69**, C1 (2004).
[4] H. W. Schäffer *et al.*, Phys. Rev. A **59**, 245 (1999).
[5] P. H. Mokler *et al.*, Phys. Rev. Lett. **65**, 3108 (1990).
[6] R. Ali *et al.*, Phys. Rev. A **55**, 994 (1997).
[7] H. W. Schäffer *et al.*, Phys. Lett. A **260**, 489 (1999).
[8] R. Marrus *et al.*, Phys. Rev. Lett. **56**, 1683 (1986).
[9] A. Derevianko and W. R. Johnson, Phys. Rev. A **56**, 1288 (1997).
[10] R. W. Dunford, Phys. Rev. A **69**, 062502 (2004).
[11] J. Rzadkiewicz *et al.*, Phys. Rev. A **74**, 012511 (2006).
[12] J. Eichler and Th. Stöhlker, Phys. Rep. **439**, 1 (2007).
[13] W. R. Nelson, H. Hirayama, and D. Rogers, computer code EGS4, SLAC Report No. SLAC-0265, 1985 (unpublished).
[14] Y. Namito and H. Hirayama, KEK Internal Report No. 2000-4, 2000 (unpublished).
[15] V. M. Shabaev *et al.*, Phys. Rev. Lett. **93**, 130405 (2004).
[16] F. James and M. Roos, Comput. Phys. Commun. **10**, 343 (1975).
[17] A. Surzhykov, P. Koval, and S. Fritzsche, Phys. Rev. A **71**, 022509 (2005).
[18] A. N. Artemyev *et al.*, Phys. Rev. A **71**, 062104 (2005).
[19] C. D. Lin *et al.*, Phys. Rev. A **15**, 154 (1977).
[20] G. W. F. Drake, Phys. Rev. A **34**, 2871 (1986).